JOURNAL OF Materials CHEMISTRY

The effect of iron on the crystalline phases formed upon thermal decomposition of Mg–Al–Fe hydrotalcites

José Maria Fernández,[a] Maria Angeles Ulibarri,[a] Francisco M. Labajos[b] and Vicente Rives*[b]

[a]*Departamento de Química Inorgánica e Ingeniería Química, Facultad de Ciencias, Universidad de Córdoba, Córdoba, Spain*
[b]*Departamento de Química Inorgánica, Universidad de Salamanca, Salamanca, Spain*

Received 26th June 1998, Accepted 5th August 1998

Layered double hydroxides (LDH) containing Mg^{II}, Fe^{III}, and Al^{III} in the brucite-like layers and interlayer carbonate (with a constant M^{II}/M^{III} ratio but varying Al^{III}/Fe^{III} ratios) have been prepared and characterised by X-ray diffraction, thermal analysis, FT-IR and UV–VIS/diffuse reflectance spectroscopies, temperature-programmed reduction and specific surface area assessment through low temperature adsorption of N_2. An Mg,Al–LDH, but with intercalated hexacyanoferrate(III), has been also prepared and characterised, in which simultaneous formation of the carbonate analogue did not occur. Thermal decomposition in air at 450 and 750 °C leads to MgO and poorly crystallised $MgFe_2O_4$ spinel (crystallinity increasing with the iron content), while for the hexacyano-containing sample, crystallization only is observed after calcination at 900 °C. This different behaviour has been related to the initial location of the iron ions.

Introduction

Layered double hydroxides (LDH) are also known as anionic clays, as they show a structure electrically opposite to that shown by clays. Their general formula is $[M^{II}_{1-x}M^{III}_{x}(OH)_2][A^{m-}]_{x/m}\cdot nH_2O$. The commonest type are the hydrotalcite group of minerals, the structure of which consists of brucite-like layers [formed by edge-sharing $Mg(OH)_6$ octahedra] with partial Mg^{II}/Al^{III} isomorphic substitution, the electrical balance being attained with carbonate anions located, together with water molecules, in the interlayer. Substitution of the layer cations is very easy, and the interlayer anion can be easily changed as well, thus giving rise to a continuous growing family of new layered materials with important applications as catalysts or catalyst precursors, sensors, anion scavengers, *etc.*[1–3]

On thermal decomposition, these materials lead to mixed oxides (also known as 'non-stoichiometric spinels'), and it has been shown[4] that the nature/structure of the solids obtained (and their applications) depend on the starting LDH which is decomposed.

The aim of the present work was to analyze how the presence of iron and its concentration in the brucite-like layers, or in the interlayer anion, may lead to solids, after calcination, with different structures. We have recently reported[4,5] on the preferential formation of $Mg_2V_2O_7$ or MgV_2O_6, with different local environments around the V^{5+} cations, from hydrotalcite-like precursors, when starting from materials containing Mg^{2+}, Al^{3+} and V^{3+} in the brucite-like layers and carbonate in the interlayer, or from materials containing Mg^{2+} and Al^{3+} in the layers and decavanadate, $V_{10}O_{28}^{6-}$, in the interlayer. In the present case, differences in location of Fe^{3+} cations in octahedral or tetrahedral sites, or different degrees of crystallinity, could be expected when Fe was in the brucite-like layer, or forming an anionic complex in the interlayer. Actually, it has been found that the crystallinity of the solids formed (or the calcination temperature required to obtain crystalline solids) depends on the precise nature of the starting LDH.

Experimental

Sample preparation

All chemicals were from Merck. For the carbonate-containing samples, a 1 M NaOH aqueous solution was added dropwise to a solution containing Mg^{2+}, Al^{3+} and Fe^{3+} nitrates in selected concentrations (ranging from 0.3 M to 0.066 M) to yield solids with different Al/Fe molar ratios, but with a constant Mg/(Al+Fe) molar ratio of 3:1, until a pH of 10 was reached, this value being maintained at constant pH (10) with a Dosimat 275 (Metrohm) coupled to a pH-meter model 691 (also from Metrohm). When addition was complete, the mixture was further magnetically stirred for 2 h. The suspension was submitted to hydrothermal treatment at autogenous pressure at 120 °C in a Teflon-lined stainless steel bomb for 24 h. The solid was then filtered and washed until nitrate and sodium ions were completely absent.

In order to prepare the hexacyanoferrate(III)-containing sample, aqueous solutions were prepared in deionised water previously boiled to remove dissolved CO_2; nitrogen was continuously bubbled through the water until it reached room temperature, after which bubbling was continued for 15 min at room temperature. Fifty ml of a 0.05 M $K_3[Fe(CN)_6]$ solution were placed in a three-necked round-bottom flask and, while magnetically stirred, 50 ml of a solution containing Mg^{2+} and Al^{3+} nitrates (0.3 M and 0.1 M, respectively) were added dropwise from a separation funnel. The same Dosimat and pH-meter cited above were used to maintain the pH at a value of 8. All of the processes were carried out at 60 °C. The suspension was left to settle overnight at room temperature and the precipitate washed with preboiled water heated to 60 °C by magnetic stirring and centrifugation, and the solid was left to dry in an oven at 80 °C in the open air.

After characterization, the samples were calcined for 2 h in air at 450 or 750 °C, in order to obtain mixed oxides. It has been previously shown[6] that the decomposition of the Mg–Al–Fe hydrotalcites is almost complete at 450 °C, and only residual hydroxyl groups are further removed between 450 and 750 °C. Labelling of the samples is given in Table 1; the calcination temperature is indicated in °C. While samples M2 to M5 and all calcined samples were ochreous, sample M6 was light yellow.

Techniques

Elemental chemical analysis for metals was carried out by atomic absorption spectroscopy (AAS) using a Perkin-Elmer 3100 apparatus after dissolution of the samples in dilute HCl.

Table 1 Labelling of the samples and elemental chemical analysis results

Sample	%Mg[a]	%Al[a]	%Fe[a]	Mg/(Al+Fe)[b]	Mg/Al[b]	Al/Fe[b]
M2	24.38	5.47	8.11	2.88		1.40
M3	24.10	3.74	9.79	3.15		0.79
M4	22.39	2.74	11.99	2.91		0.47
M5	22.86	—	17.92	2.93		—
M6	18.73	6.56	4.99		3.17	2.73
M2–450	28.68	6.12	8.74	3.08		1.45
M3–450	26.90	4.50	11.49	2.96		0.81
M4–450	26.19	3.14	13.51	3.01		0.48
M5–450	27.46	—	19.37	3.25		—
M6–450	23.76	8.26	5.56		3.19	3.09
M2–750	32.15	7.29	10.21	2.92		1.48
M3–750	28.02	5.04	11.91	2.88		0.88
M4–750	27.04	3.58	14.62	2.82		0.51
M5–750	32.62	—	23.48	3.19		—
M6–750	25.38	8.93	6.38		3.16	2.90

[a]Weight percentage. [b]Molar ratio, *x*:1.

Carbon and nitrogen were analyzed in sample M6 in a Perkin Elmer 2400 CHN analyzer.

Powder X-ray diffraction (PXRD) diagrams were recorded on a Siemens D500 instrument, using graphite-filtered Cu-Kα radiation ($\lambda = 1.54050$ Å); the instrument was equipped with a DACO-MP microcomputer, and software Diffract-AT was used to analyze the data, identification of existing crystalline phases being concluded from comparison with JCPDS diffraction files. In some cases, where small amounts of sample were available, an Al sample holder was used, and thus, sharp, intense diffraction peaks due to the holder were recorded, but these peaks were unambiguously identified.

Differential thermal analysis (DTA) and thermogravimetric analysis (TG) were recorded on Perkin-Elmer DTA1700 and TGS-2 instruments, respectively, using flowing air (60 ml min^{-1}) at a heating rate of 12 °C min^{-1}.

Fourier-transform infrared spectra (FT-IR) were recorded using the KBr pellet technique on a Perkin-Elmer FTIR-1730 instrument; one hundred scans were averaged in order to improve the signal-to-noise ratio, and the nominal resolution was 4 cm^{-1}.

Ultraviolet–visible (UV–VIS) spectra were recorded following the diffuse reflectance (DR) technique in a Shimadzu UV-240 instrument, using MgO as reference and a slit of 5 nm.

Specific surface area and porosity of the samples were determined on a Gemini instrument from Micromeritics. The samples were previously degassed at 125 °C for 2 h with nitrogen in a Micromeritics FlowPrep 060 apparatus. The adsorption–desorption isotherms (−196 °C) were analyzed using literature software.[7]

Temperature-programmed reduction (TPR) runs were performed in a TPR/TPD 2900 instrument from Micromeritics, using a 5% H_2/Ar (vol.) mixture to reduce the samples. Amounts of samples of *ca.* 15 mg were used, and the gas flow, sample weight and heating rate were chosen in order to attain good resolution of the reduction peaks.[8] The gas, at the reactor exit, was passed through a cold trap (melting isopropanol) to retain vapours and condensable gases before entering the detector.

Results and discussion

Elemental chemical analysis

The results obtained for Mg, Al and Fe are given in Table 1; the calculated M^{II}/M^{III} and Al/Fe ratios are also given. C and N were analyzed for sample M6, obtaining values of 6.3 and 6.8%, respectively. The average M^{II}/M^{III} ratio, *i.e.*, the ratio between the molar fraction of divalent and trivalent cations in the layers, $Mg^{2+}/(Al^{3+}+Fe^{3+})$, was 2.97:1 for samples M2 to M5; for sample M6 the Mg^{2+}/Al^{3+} ratio was 3.17:1; these two values are acceptably close to the expected value existing in the starting solutions (3:1). On the other hand, the Al/Fe ratio for sample M6 was 2.73:1. The expected value for this ratio was 3:1, as the negative charge of the interlayer anion should balance the positive charge due to Al^{3+} in the layers, and so, the anion existing in this sample [hexacyanoferrate(III)] being trivalent, a value of 3:1 would be expected.

If hexacyanoferrate(III) is the only anion existing in sample M6, then the ratio between the weight percentages of C and N would be 0.86:1; however, the experimental value was 0.93:1, indicating that a slight excess of carbon exists. From the FT-IR results (see below) the presence of a small amount of carbonate species, probably adsorbed on the external surface of the crystallites, can be concluded, thus explaining this finding, as formation of a co-product containing intercalated carbonate was not observed (see powder X-ray diffraction results below). On the other hand, the molar N/Fe ratio is very close to the expected value (6:1).

Powder X-ray diffraction

The diagrams for the original samples are shown in Fig. 1. They are all similar, with sharp bands at low 2θ values, corresponding to the higher order 001 reflections of a layered material. The sharp peaks recorded for sample M3 close to $2\theta = 38$ and 45° superimposed to broader maxima (also recorded in the same positions for the other samples), and that recorded at $2\theta = 65°$ are due to the Al sample holder. The positions of the harmonics are coincident for samples M2, M3, M4, and M5, while for sample M6 these harmonics are shifted towards lower 2θ values (*i.e.*, larger spacings). Assuming a 3R polytypism,[9] the first (from low 2θ values) peaks can be indexed as (003), (006), and (009), and from their positions, the values for parameter *c* have been calculated (Table 2) as $c = [d(003) + 2\,d(006) + 3\,d(009)]$.

The values for parameter *a* (which coincides with the average cation–cation distance in the brucite-like layers) are also included in Table 2, and have been calculated from the position of the peak due to planes (110), which is the first peak of the doublet recorded close to $2\theta = 60°$, as $a = 2\,d(110)$. It should be noted that for samples M2 to M5, a steady increase in *a* is observed. This is due to the progressive Al^{3+}/Fe^{3+} substitution (see elemental chemical analysis data in Table 1), and the larger ionic radius of Fe^{3+} (78.5 pm in high spin, octahedral coordination) than Al^{3+} (67.5 pm in octahedral coordination).[10] This is also the reason of the lower *a* value for sample M6, where the only trivalent cation in the layers is Al^{3+}.

The slight differences in the values of parameter *c* for

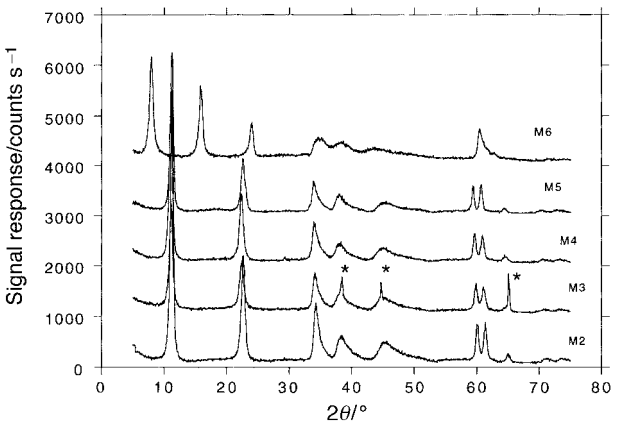

Fig. 1 Powder X-ray diffraction profiles for samples M2 to M6. (*) signals due to the Al sample holder. The traces have been displaced vertically for clarity.

Table 2 Summary of X-ray diffraction results, specific surface area determination and temperature-programmed reduction

Sample	c/Å	a/Å	S_{BET}/m^2 g^{-1}	H_2/Fe[a]
M2	23.52	3.08	59	1.36
M3	23.73	3.09	68	1.68
M4	23.82	3.10	70	1.42
M5	23.67	3.11	48	1.25
M6	33.36	3.06	143[b]	—
M2–450			123	1.40
M3–450			145	1.56
M4–450			138	1.63
M5–450			81	1.67
M6–450			123	1.68
M2–750			101	1.12
M3–750			113	1.22
M4–750			117	1.43
M5–750			16	1.35
M6–750			110	1.28

[a]Molar ratio, x:1. [b]128 m^2 g^{-1} surface area equivalent to adsorption on micropores, and 15 m^2 g^{-1} external surface area.

samples M2 to M5 [the higher value for sample M6 is due to the presence of hexacyanoferrate(III) instead of carbonate] cannot, however, be easily related to particular differences in the samples, as the small changes observed could be due to small differences in the hydration degree of the interlayer. From the thickness of the brucite-like layers, 4.8 Å,[3] the interlayer space for the carbonate-containing samples is close to 3 Å, corresponding to carbonate anions with their molecular plane parallel to the brucite-like layers.

With regards to sample M6, it should be stressed that no peak has been recorded which could be ascribed to the presence of a co-product corresponding to carbonate-interlayered hydrotalcite. This result is extremely important, as in most of the papers previously reported in the literature on hexacyanoferrate-containing layered double hydroxides,[11–13] co-formation of a carbonate–LDH, together with that of the hexacyanoferrate form, is usually observed. The gallery height [from the spacing for planes (003), 11.12 Å, and the thickness of the brucite-like layers, 4.8 Å] was 6.32 Å. The size of the $Fe(CN)_6^{3-}$ anion is close to 11 Å along the C_4 axis, 8.7 Å along the C_2 axis, and 6.5 Å along the C_3 axis.[14] This means that the anion should be oriented with its C_3 axis (that joining parallel faces of the octahedron) perpendicular to the brucite-like layers and that, even so, some stress and distorsion should exist. Alternatively, grafting of the anion to the brucite-like layers, in a similar way to that previously described for several vanadates intercalated in LDHs,[15,16] could be claimed.

The PXRD diagrams of the samples calcined at 450 and 750 °C are included in Fig. 2. Again, sharp peaks due to the Al sample holder are recorded in some cases. With regard to the maxima of the samples, these are extremely broad and their positions roughly coincide for all five samples calcined at 450 °C, while for samples calcined at 750 °C the PXRD diagram of sample M6-750 is rather similar to those recorded for the samples calcined at 450 °C; on the contrary, for samples M2-750 to M5-750 a progressive increase in the intensity of new, sharper peaks (not recorded for samples calcined at 450 °C) is observed.

For a hydrotalcite structure to remain stable, the M^{II}/M^{III} ratio should be larger than 1:1.[2] Calcination of hydrotalcites leads to removal of volatile interlayer anions and hydroxyl groups, and formation of the corresponding oxides, usually $M^{II}O$ and the $M^{II}M^{III}_2O_4$ spinel, although observation of diffraction peaks due to the crystalline spinel depends on the nature of the metal cations and on the calcination temperature (*e.g.*, crystalline Mg,Al spinel is only detected after calcination at *ca.* 900–1000 °C).[17,18] The pure spinel cannot be obtained, unless redox processes simultaneously occur during calcination, as the M^{II}/M^{III} ratio in the spinel is equal to 0.5:1, and so crystallization of $M^{II}O$ is always observed.[19,20] Additionally, some diffraction peaks of MgO are recorded almost coincident with diffraction peaks of spinels.

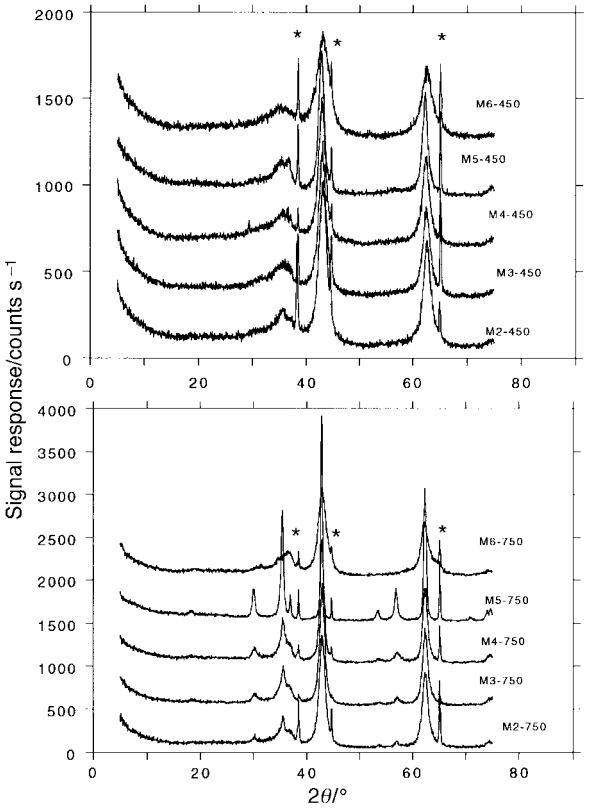

Fig. 2 Powder X-ray diffraction profiles for samples M2 to M6 calcined at (upper) 450 and (lower) 750 °C for 2 h. (*) signals due to the Al sample holder. The traces have been displaced vertically for clarity.

With this, taking into account the nature of the cations existing in our samples, the following phases could be formed: MgO, $MgAl_2O_4$, $MgFeAlO_4$, $MgFe_2O_4$. The presence of MgO is concluded in all ten cases from the two intense peaks at 2.10 and 1.48 Å (*ca.* $2\theta = 43$ and 63°, respectively), and the excess in MgO above the stoichiometric amount required to form any Mg-containing spinel.

From the positions of the peaks in the PXRD diagram of sample M5-750 (where the sharpest peaks are recorded), excluding the peaks coincident with those of MgO, the cell dimension for the spinel formed can be calculated as 8.402 Å. The reported values[21] for other spinels are 8.083 Å ($MgAl_2O_4$, JCPDS file 21-1152), 8.320 Å ($MgFeAlO_4$, JCPDS file 11-9), 8.387 Å ($MgFe_2O_4$, JCPDS file 36-398), and 8.396 Å (Fe_3O_4, JCPDS file 19-629). From comparison between the reported and the calculated values it can be concluded that the spinel formed in our samples should be $MgFe_2O_4$. We want to stress that the Al sample holder behaves in our case as a sort of 'internal reference', for better definition of the positions of the peaks. In addition, formation of Fe_3O_4 can be tentatively assumed, if $Fe^{3+} \rightarrow Fe^{2+}$ reduction could take place during calcination in air.

So, the PXRD data for the calcined samples can be summarized as follows: calcination at 450 °C gives rise, in all cases, to formation of ill-crystallized MgO, and a small amount of a $MgFe_2O_4$ spinel. When the calcination temperature is increased to 750 °C the presence of the spinel is more evident, especially in the case of sample M5-750 (that is, that without aluminium and with the largest Fe content), while for sample M6-750 (prepared from the hexacyanoferrate precursor) the diagram is almost coincident with that recorded for the same

sample, but calcined at 450 °C, indicating that crystallization of the spinel has not been favoured, or it is not detected due to the low Fe content (see Table 1). This conclusion can be easily reached from comparison of the intensity of the peak close to $2\theta = 57°$ ($d = 1.615$ Å), corresponding to planes (511) or (333) of $MgFe_2O_4$. Its intensity increases steadily from sample M2-750 to sample M5-750, but the peak is absent in the diagram of sample M6-750. As for calcination of a Mg,Al hydrotalcite in this same temperature range, no crystalline phase containing Al has been observed.[22,23]

In order to gain insight into the formation of crystalline phases, selected samples have been calcined at higher temperatures or for longer periods of time. When sample M4 is calcined at 750 °C for 4, 8 or even 24 h, instead of 2 h as used for the sample whose PXRD diagram is shown in Fig. 2, the only effect observed is a slight sharpening of the diffraction peaks due to the spinel. The effect is even less evident for sample M5 calcined for these periods of time at 750 °C, as in this sample, calcination for 2 h is enough to form the spinel, as shown by the sharp peaks recorded (Fig. 2). With regards to sample M6, calcination at 750 °C for even 24 h has only minor effects on the PXRD diagram, and only peaks due to MgO, and broad, ill-defined peaks due to the $MgFe_2O_4$ spinel, are again recorded.

However, when sample M6 was calcined at higher temperatures, the changes were rather drastic. Fig. 3 includes the PXRD diagrams for this sample calcined at 450, 750, 900, 1000, and 1100 °C for 2 h. From 900 °C upwards, the diffraction peaks due to the spinel are clearly observed, although some of them coincide with peaks due to MgO.

Thus, we can conclude that the lack of detection of peaks due to the spinel in sample M6-750 is not due to the low sensitivity of the technique, as calcination at higher temperature gives rise to samples where the peaks due to the spinel are clearly detected. In other words, the lack of formation of the $MgFe_2O_4$ spinel in sample M6-750, even though the spinel is formed in all other samples calcined for 2 h at this same temperature, is undoubtedly related to the different location of the Fe(III) ions in these two series of samples: in the layers (samples M2 to M5) or in the interlayer space, as hexacyanoferrate (sample M6).

Differential thermal analysis (DTA) and thermogravimetric analysis (TG)

Representative TG and DTA curves for selected samples are shown in Fig. 4. Weight loss starts from room temperature and is completed at *ca.* 750 °C. Two steps are observed, as is usual for hydrotalcites.[24] The first one, up to *ca.* 200–250 °C, corresponds to removal of water physisorbed on the external

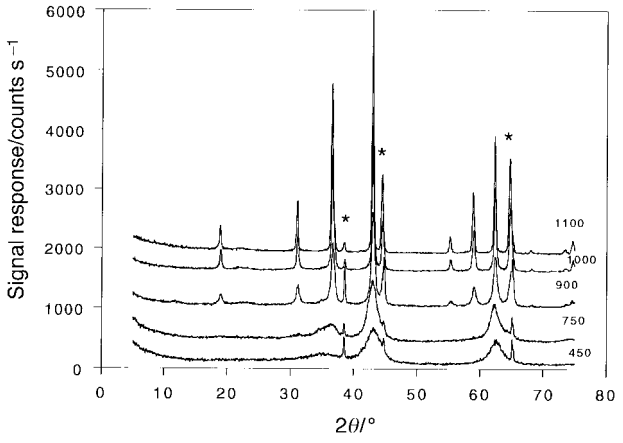

Fig. 3 Powder X-ray diffraction profiles for sample M6 calcined for 2 h at the temperatures given (in °C). (*) signals due to the Al sample holder.

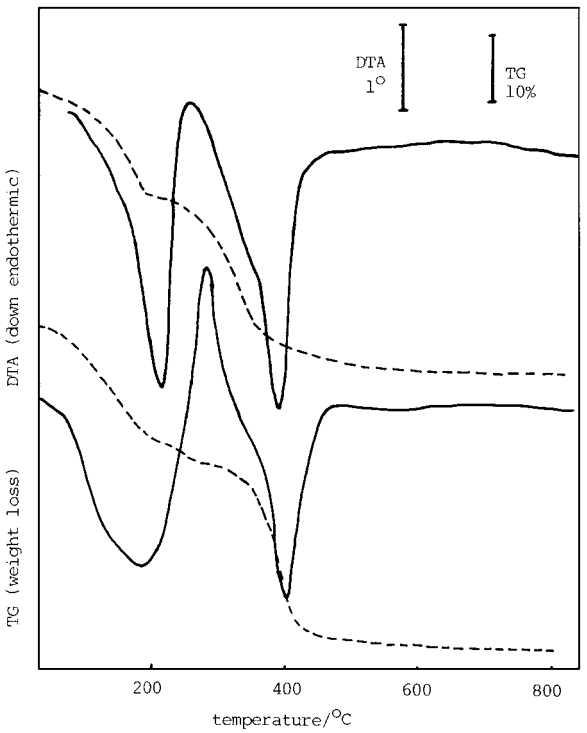

Fig. 4 Thermogravimetric (dotted lines) and differential thermal (solid lines) analyses for samples M5 (upper traces) and M6 (lower traces).

surface of the particles, and water molecules from the interlayer space, and amounting to *ca.* 15% of the initial weight of the sample. The second weight loss is almost completed at *ca.* 450 °C, and corresponds to removal of hydroxyl groups from the brucite-like layers, as well as of volatile species from the interlayer anions (*i.e.*, CO_2 from interlayer carbonate), as concluded in previous studies[25] on a Mg,Al–carbonate hydrotalcite. The weight loss above 450 °C amounts to *ca.* 1–2% of the initial sample weight, and is usually ascribed to removal of strongly held hydroxyl groups. From the elemental chemical composition of the starting solid (Table 1) and the total weight loss up to 750 °C, assuming formation of mixed oxides (MgO, Fe_2O_3 and Al_2O_3, or any combination of these) at the highest temperature reached, the interlayer water content can be calculated, thus providing the whole formula of the starting layered materials (Table 3). The behaviour shown by sample M6 is slightly different and even though decomposition was essentially complete at the same temperature (about 750 °C), intermediate decomposition steps can be observed; unfortunately, we were unable to analyze the gases evolved during decomposition, to assess the different decomposition steps.

The maximum number of water molecules hosted in the interlayer space of a carbonate-containing hydrotalcite can be easily calculated.[26,27] Water molecules and interlayer carbonate anions can be close-packed in the interlayer region, as hydroxyl groups are in the brucite-like layers. We can assume the size of a water molecule to be coincident with that of a hydroxyl group and about one third of that of a carbonate anion. If these are located with their molecular plane parallel to the

Table 3 Formulae of the samples prepared

Sample	Formula[a]
M2	$[Mg_{0.74}Fe_{0.11}Al_{0.15}(OH)_2][CO_3]_{0.13}\cdot 0.70H_2O$
M3	$[Mg_{0.76}Fe_{0.13}Al_{0.11}(OH)_2][CO_3]_{0.12}\cdot 0.69H_2O$
M4	$[Mg_{0.75}Fe_{0.17}Al_{0.08}(OH)_2][CO_3]_{0.13}\cdot 0.69H_2O$
M5	$[Mg_{0.75}Fe_{0.25}(OH)_2][CO_3]_{0.13}\cdot 0.61H_2O$
M6	$[Mg_{0.76}Al_{0.24}(OH)_2][Fe(CN)_6]_{0.08}\cdot 0.83H_2O$

[a]The values have been rounded to the nearest 0.01.

layers (as concluded from the width of the interlayer space, from the spacing determined by PXRD), then the maximum number of water molecules would be $2-(3x/2)$ per hydrotalcite 'formula', where x stands for the molar fraction of trivalent cations in the brucite-like layers. In our case $x \approx 0.25$, and then up to 1.6 water molecules can be located. The experimental value is lower, probably because the preferred orientations maximize hydrogen bonding.

The DTA curves, shown in Fig. 4, are qualitatively coincident with those previously reported for different hydrotalcite-like materials,[23,24,28] with two endothermic effects corresponding to the weight losses above described. Despite the differences between the samples studied, the effects are recorded at almost coincident temperatures, 205–230 and 405 °C, and should correspond to the two weight losses recorded in the TG curves. In all cases, a shoulder at *ca.* 365 °C is also recorded. Between both effects, an exothermic effect is observed at *ca.* 310 °C for sample M6, although it is absent in the curves for the other samples. It is clearly an exothermic effect, and not an instrumental artifact (the other DTA curves also show a 'maximum' in this position), because the signal grows above the baseline of the curve. We tentatively ascribe this effect to combustion of the cyanide ligands under the oxidizing atmosphere used during the DTA.

FT-IR spectroscopy

This technique has been used mainly to identify the interlayer anions in the samples studied.

The spectra for samples M2, M5, and M6 are shown in Fig. 5. These samples have been selected as, due to their chemical composition, differences among their FT-IR spectra are expected to be more evident than those for samples M3 and M4.

The broad band centered around 3500 cm^{-1} is due to the stretching mode of hydroxyl groups, both those in the brucite-like layers and from the interlayer water molecules; the broadness of the band indicates that hydrogen bonds with a wide range of strength exist. Hydrogen bonding of interlayer water molecules to interlayer carbonate anions has been claimed[23,29] to be the origin of the broad, very weak shoulder recorded slightly above 3000 cm^{-1}, absent in the spectrum of sample M6, in agreement with the lack of interlayer carbonate in this sample. The medium band at 1636 cm^{-1} is due to the deformation mode of water molecules, and the bands below 1000 cm^{-1} are due to M–O vibration modes; the presence of different amounts of Mg^{2+}, Al^{3+} and Fe^{3+} in the brucite-like layers in the different samples would account for the different relative intensities of these bands in the different spectra.

The absorption around 1370–1390 cm^{-1} is clearly composed of two superimposed bands for samples M2 and M5, a very sharp band (also recorded for sample M6) at 1381 cm^{-1}, and a broader band at 1374 cm^{-1}. This last band is due to mode ν_3 of the interlayer carbonate anions. The shift from the position reported[30] for free carbonate is due to restricted freedom and hydrogen bonding (as concluded from the broad absorption just above 3000 cm^{-1}) in the interlayer region. This band could be argued to be present (although very much weaker) in the spectrum of sample M6. However, other experimental data here described (absence of PXRD diffraction maxima close to 7.8 Å, characteristic of carbonate-interlayered hydrotalcites, and the lack of the FT-IR absorption slightly above 3000 cm^{-1}) strongly suggest that interlayer carbonate anions do not exist in this sample, and so this band could be due to the presence of carbonate species weakly adsorbed on the external surface of the crystallites, taking into account the strong basiticy of these solids and that the samples are exposed to atmosphere during manipulation to record the spectra. The sharp band at 1381 cm^{-1} is due to a nitrate impurity existing in the KBr used to prepare the discs as it is also present in the pure KBr discs.

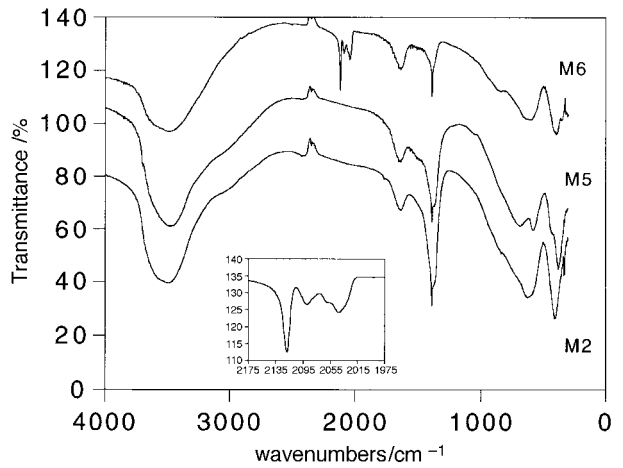

Fig. 5 FT-IR spectra of samples M2, M5, and M6. Inset: spectrum of sample M6 in the 2175–1975 cm^{-1} range.

Another set of bands is recorded between *ca.* 2200–2000 cm^{-1} for sample M6. This constitutes a 'window' in the spectral range, where, in the samples here studied, only the bands due to the C–N stretching of cyanide groups are expected. For hexacyanoferrate, the exact position of the band depends on the oxidation state of iron,[31] and for reference potassium hexacyanoferrate(III) the band was recorded at 2118 cm^{-1}. This band is the most intense one recorded in this range, but, in addition, a weak band is recorded at 2042 cm^{-1}, with even weaker shoulders at 2089 and 2060 cm^{-1}. The ν_{CN} band of potassium hexacyanoferrate(II) is recorded at 2044 cm^{-1}, suggesting that a partial $Fe^{3+} \rightarrow Fe^{2+}$ reduction has taken place in the sample studied here. This reduction process has been previously claimed by several authors to occur upon intercalation of hexacyanoferrate(III) in different hydrotalcites, as well as oxidation of hexacyanoferrate(II).[11,12,32–36] It has been also reported that the $Fe^{3+} \rightarrow Fe^{2+}$ reduction can take place under high pressure,[37,38] and, actually, the sample was submitted to high pressure to prepare the KBr disc. However, such multiple absorptions in this wavenumber range were also recorded when the spectrum was recorded by the DRIFTS technique (diffuse reflectance IR FT spectroscopy), without application of any sort of pressure. Nevertheless, if such a reduction is assumed (and hexacyanoferrate anions are known to be outer-sphere electron-transfer reductants or oxidants[39,40]), the origin of the other two weaker bands at 2089 and 2060 cm^{-1} can be easily explained. According to Jones,[41] the A_{1g}, E_g and T_{1u} ν_{CN} modes required by the O_h point group for $Fe(CN)_6^{4-}$ are recorded at 2094, 2062 and 2044 cm^{-1} in aqueous solution, the first two bands being infrared-forbidden, but in the interlayer space of the hydrotalcite surely become partially activated by a decrease in symmetry, here being recorded at 2089 and 2060 cm^{-1}, respectively. If grafting has occured [as it could be concluded from a calculated gallery height smaller than the size of the $Fe(CN)_6^{3-}$ moiety along the C_3 axis], the decrease in symmetry would be much more drastic and the spectrum much more complicated. So, we may conclude that partial $Fe^{3+} \rightarrow Fe^{2+}$ reduction has taken place because of the stress generated in the hexacyanoferrate(III) anion between the close brucite-like layers.

Ultraviolet–visible/diffuse reflectance spectroscopy

The results obtained for samples M2 to M5 (as well as for the corresponding calcined samples) were rather similar, but discussion will be centered on sample M5, with the highest iron content. As expected, the behaviour shown by sample M6 was different.

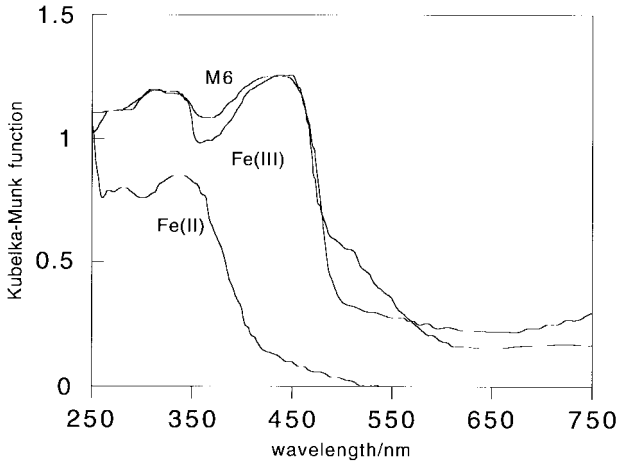

Fig. 6 UV–VIS/DR spectra of sample M6 and of potassium hexacyanoferrate(II) and hexacyanoferrate(III).

The spectrum for sample M5 shows a broad absorption extending from 700 nm to lower wavelength, centered at *ca.* 400 nm, and with a sharp absorption close to 300 nm. As Mg^{2+} and Al^{3+} have d^0 configurations and Fe^{3+} has a d^5 high-spin configuration (due to weak field oxide ligands), the expected absorptions should be exclusively due to charge transfer processes from the oxide ligands to the Fe^{3+} ions. When the sample is calcined at 450 °C the absorption becomes broader, with only minor changes in the spectrum of the sample calcined at 750 °C. No important difference is, however, observed in the colour (brown) of the sample prior to or after calcination.

The spectrum recorded for sample M6 (the sample is yellow) is shown in Fig. 6. For comparison, the spectrum of commercial potassium-hexacyanoferrate(III) and -hexacyanoferrate(II) (existing in this sample, according to the FT-IR results above discussed), are included in the same figure. $[Fe(CN)_6]^{3-}$ shows a broad absorption centered at 460 nm, and a structured absorption at 315 nm. On the other hand, $[Fe(CN)_6]^{4-}$ shows an absorption at *ca.* 330 nm. The origin of these bands has been discussed for model hexacyanometalate compounds by Gray and co-workers.[42,43] In the hexcacyanoferrate(III) compound there is a spin-allowed transition (d^5 configuration, low spin octahedral coordination), responsible for the absorption around 450 nm, while absorptions at lower wavelengths and in the hexacyanoferrate(II) compound (d^6 configuration, low spin octahedral coordination) are due to ligand/metal charge transfer processes. The spectrum of sample M6 shows two absorptions at 460 and 315 nm, coinciding with those of the $[Fe(CN)_6]^{3-}$ species, but the 'valley' between these two absorptions, close to 330 nm, is less pronounced, this probably being due to the presence of $[Fe(CN)_6]^{4-}$. Altogether, these results further confirm that the structure of the hexacyanoferrate moiety is mostly maintained after incorporation into the interlayer space of the hydrotalcite material.

Upon calcination, the colour of samples M6-450 and M6-750 becomes brown, and their spectra are almost coincident with those recorded for the other samples calcined at the same temperatures. These results indicate that, upon calcination and destruction of the layered structure, the local environment of the iron ions becomes almost the same (if not identical) in all samples.

Specific surface area measurements

The specific surface areas of the samples, as determined from the nitrogen adsorption isotherms at −196 °C, are given in Table 2. For original samples M2 to M5 the isotherms belong to type II in the IUPAC classification,[44] and correspond to unrestricted adsorption. The specific surface area values increase from sample M2 to sample M4, but decreases for sample M5. These differences can be readily related to the different crystallinity of the samples, as concluded from the sharpness and half-width of the main diffraction maxima recorded in the PXRD patterns.

The value for sample M6 is extremely large, and its adsorption–desorption isotherm corresponds to type I in the IUPAC classification, characteristic of adsorption on microporous solids. These findings are similar to those previously reported by Cavalcanti *et al.*[34] for hexacyanoferrate-containing hydrotalcites. According to these results, the nitrogen molecules are not able to enter into the interlayer space of the carbonate-containing hydrotalcites, but enter into the interlayer of the hexacyanoferrate hydrotalcites. The reason for this different behaviour should be in the population of the interlayer space, and probably in the size of the gallery (*ca.* 3 Å for the carbonate-containing samples, but 6.32 Å for sample M6). Anions and water molecules exist in the interlayer between the brucite-like sheets. The role of the anions is to balance the electric positive charge of the layers (originated by the M^{2+}/M^{3+} exchange) and, as the formal negative charge of the anions increases, a lower number of anions are required for a given positive charge to be balanced. In our case, the M^{2+}/M^{3+} ratio is *ca.* 3:1 in all cases, but the formal charge of the anions is −2 for samples M2 to M5 and −3 for sample M6. With this, despite the larger size of the hexacyanoferrate anion, more room would be available to host nitrogen molecules in sample M6 than in samples M2 to M5. Moreover, the swelling of the structure upon incorporation of the larger hexacyanoferrate anion (from gallery heights *ca.* 3 Å for carbonate-containing hydrotalcite to 6.32 Å for the hexacyanoferrate form) will also facilitate nitrogen insertion into the interlayer space.

When the samples are calcined at 450 and 750 °C, the layered structure is destroyed (see PXRD data above) and the differences in the specific surface areas (Table 2) cannot be related to the layered structure, but simply to the different crystallinity of the samples. For samples M2 to M5, an increase is observed from the values for the original samples to those for the samples calcined at 450 °C, due to formation of less crystalline, mostly amorphous phases; among those samples calcined at 450 °C, the PXRD peaks of sample M5-450 are much sharper than for the other samples calcined at 450 °C, thus indicating a more crystalline material, *i.e.*, with a lower specific surface area, as experimentally observed. On heating at 750 °C, the values decrease from those obtained at 450 °C in most of the cases, the behaviour shown by sample M5-750 (without aluminium) being noticeable, with a specific surface area of 16 $m^2\ g^{-1}$ only, probably due to formation of the well crystallized spinel structure, see PXRD results in Fig. 2. Again, the behaviour shown by sample M6 is singular, with specific surface areas close to 110–120 $m^2\ g^{-1}$ in agreement with the rather amorphous structure of this material, as concluded from PXRD measurements, and of the same order as those for samples M2 to M4, even after calcination at 750 °C.

Temperature-programmed reduction

The technique was used in order to analyze the way Fe^{3+} is reduced in the samples. However, it should be taken into account that the sample is being decomposed simultaneously with the reduction as the temperature is increased during the TPR runs, and so the results obtained cannot be simply related to reduction of cations as they were in the original materials.[45] On the other hand, it has been observed in some cases that reduction has not been completed (*i.e.*, the curve does not recover the baseline) even at the maximum temperature attainable by the instrument, and so a full quantitative analysis has not been performed, although hydrogen consumptions are given in Table 3.

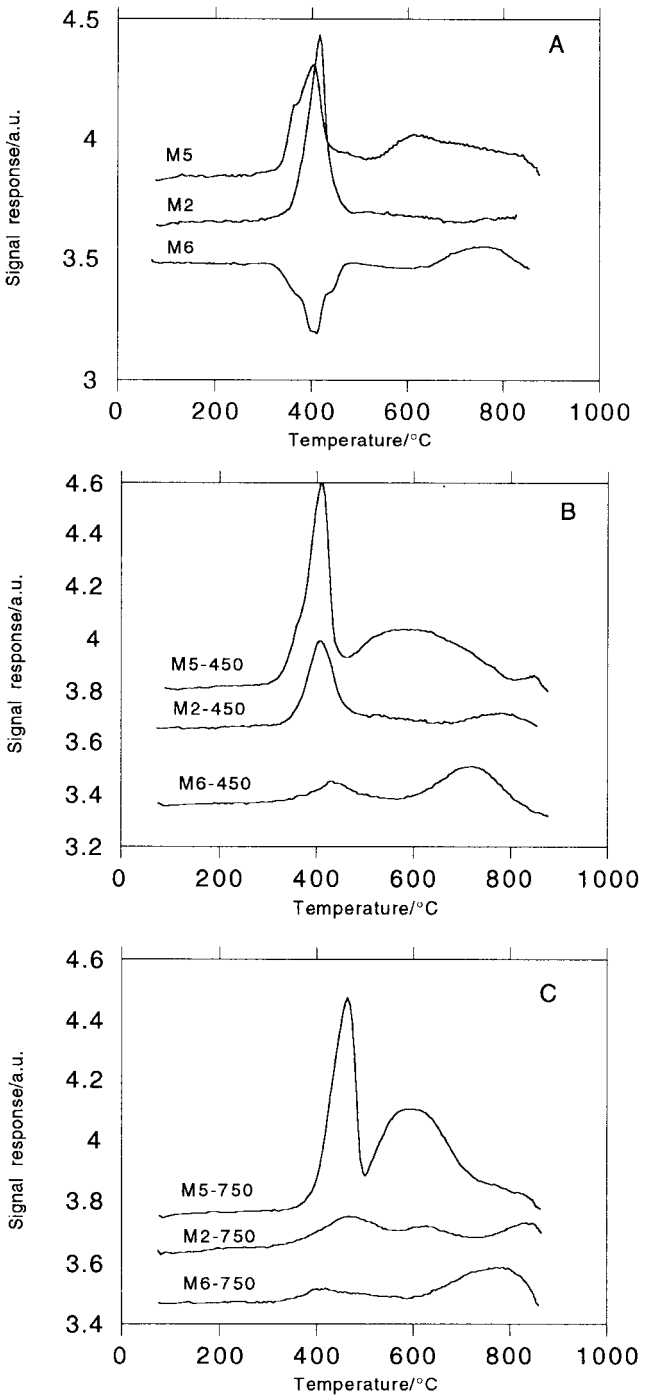

Fig. 7 Temperature-programmed reduction profiles of samples M2, M5, and M6. (A) Original samples; (B) calcined at 450 °C; (C) calcined at 750 °C.

The curves for samples M2, M5 and M6 are shown in Fig. 7A. While for sample M2 a single reduction peak, with a maximum at 416 °C (close positions are observed for the other carbonate-containing hydrotalcites, and the peak becomes slightly broader), is recorded, a second, broader, peak, incomplete for sample M5, is recorded for the other carbonate-containing samples. The molar H_2/Fe ratio was in all cases fairly close to the expected value of 1.5:1, for total reduction from Fe^{3+} to Fe^0 (PXRD analysis of the residue after the TPR run of sample M4 indicates formation of metallic Fe). However, such a ratio was only 1.25:1 for sample M5, in whose TPR profile the baseline has not been recovered even at 850 °C, the maximum temperature attainable by our experimental system for TPR analysis.

The profile for sample M6 is completely different. In addition to a broad peak at 758 °C, it shows also a 'negative' peak at 404 °C, undoubtedly due to removal of cyanide ligands during decomposition. It should be remembered that the TPR curve is obtained from a chromatographic analysis of the gas after the sample (where the concentration of H_2 has decreased because of reduction), and thus, the presence of other gases (from cyanide decomposition) would account for unexpected changes in the conductivity. Thermogravimetric analysis has shown that these ligands are removed below 450 °C, and, unfortunately, reduction takes place in the same temperature range.

The curves for the samples calcined at 450 °C are included in Fig. 7B. A sharp reduction peak is again recorded at 410 ± 6 °C for samples M2-450 to M5-450, together with a weaker, broader feature at higher temperatures; reduction was not complete at 850 °C. However, for sample M6-450, two reduction peaks were recorded at 432 and 719 °C, and it should be noted that the relative intensities of the high/low reduction peaks is reversed for sample M6-450, if compared with the other samples.

Different peaks in a TPR profile where a single cation is reduced can be ascribed to consecutive reduction steps (*e.g.*, $Fe^{3+} \rightarrow Fe^{2+}$, and $Fe^{2+} \rightarrow Fe^0$), or to reduction of different species (*e.g.*, reducible crystals differing in their size or dispersion, or cations in different environments) in a single step, or even a mixing of both. In the first case, the ratio between the integrated areas of the peaks (directly related to hydrogen consumption) should be constant (*e.g.*, for $Fe^{3+} \rightarrow Fe^{2+}$ and $Fe^{2+} \rightarrow Fe^0$, it should be 0.5:1). So, in the present case, the change in relative intensities of the peaks recorded for sample M6-450 (ex-hexacyanoferrate) should correspond to the presence in this sample of species with a different dispersion/reducibility than in the samples prepared from hydrotalcites with Fe^{3+} ions in the brucite-like layers.

The behaviour shown by the samples calcined at 750 °C, Fig. 7C, is rather similar to those of the samples calcined at 450 °C: A fairly sharp peak, now at 464 ± 4 °C, followed by a broader, sometimes structured, peak extending from *ca.* 600–800 °C. On the contrary, two peaks (with reversed relative intensities) were recorded for sample M6-750, centered at 412 and 778 °C, a similar profile to that recorded for sample M6-450.

Conclusions

In this paper, we have prepared hyrotalcite-like materials with a given M^{II}/M^{III} ratio (M^{II} = Mg; M^{III} = Al, Fe), but varying the ratio between two trivalent cations (Al/Fe) in the layers. We have also prepared a sample with the same structure, but containing hexacyanoferrate(III) in the interlayer space, without simultaneous co-formation of a carbonate-intercalated material, although hexacyanoferrate(II) is partially formed. The solids have been characterised, and their thermal behaviour analyzed. It has been found that, despite thermal decomposition in air leading in all cases to a mixture of MgO and $MgFe_2O_4$, the crystallinity depends both on the calcination temperature, and on the Al/Fe ratio and on the initial location of the Fe^{III} ions: at 450 °C all samples are mostly amorphous, and poorly crystallized MgO is formed. At 750 °C, additional crystallization of $MgFe_2O_4$ is observed in the ex-carbonate samples, and especially in the absence of Al; however, in the ex-hexacyanoferrate sample the crystalline phases existing are the same as after calcining at 450 °C. Prolonging the calcination time from 2 to 24 h or raising the calcination temperature has only minor effects on the crystallinity of the species formed. For the ex-hexacyanoferrate sample, however, spinel $MgFe_2O_4$ formation is only detected above 900 °C.

These results show that the initial location of the Fe^{III} ions is of paramount importance in determining the nature of the crystalline phases formed, depending on the calcination tem-

perature, and thus will hopefully determine their use as catalysts or magnetic materials.

Authors thank Dr. B. Macías and Mr. A. Montero (University of Salamanca), and Ms. F. Pérez-Taboada (University of Córdoba) for their assistance in obtaining some of the experimental results. Financial support from Junta de Andalucía (group FQM-214) and Ministerio de Educación y Ciencia (PB96-1307-C03) is also acknowledged.

References

1 A. de Roy, C. Forano, K. El Malki and J. P. Besse, in *Expanded Clays and Other Microporous Solids*, eds. M. L. Occelli and H. E. Robson, Van Nostrand Reinhold, New York, 1992, p. 108.
2 F. Trifirò and A. Vaccari, in *Comprehensive Supramolecular Chemistry*, eds. J. L. Atwood, J. E. D. Davies, D. D. MacNicol, F. Vögtle, J.-M. Lehn, G. Alberti and T. Bein, Pergamon-Elsevier Science, Oxford, 1996, vol. 7, p. 251.
3 F. Cavani, F. Trifirò and A. Vaccari, *Catal. Today*, 1991, **11**, 1.
4 F. Kooli, I. Crespo, C. Barriga, M. A. Ulibarri and V. Rives, *J. Mater. Chem.*, 1996, **6**, 1199.
5 F. M. Labajos, V. Rives, P. Malet, M. A. Centeno and M. A. Ulibarri, *Inorg. Chem.*, 1996, **35**, 1154.
6 R. Trujillano, Ph.D. Thesis, University of Salamanca, Spain, 1997.
7 V. Rives, *Adsorpt. Sci. Technol.*, 1991, **8**, 95.
8 P. Malet and A. Caballero, *J. Chem. Soc., Faraday Trans.*, 1988, **84**, 2369.
9 A. S. Bookin and V. A. Drits, *Clays Clay Miner.*, 1993, **41**, 551.
10 J. E. Huheey, E. A. Keiter and R. I. Keiter, *Inorganic Chemistry: Principles of Structure and Reactivity*, Harper Collins, New York, 4th edn., 1993.
11 M. J. Holgado, V. Rives, M. S. Sanromán and P. Malet, *Solid State Ionics*, 1996, **92**, 273.
12 H. C. B. Hansen and C. B. Koch, *Clays Clay Miner.*, 1994, **42**, 170.
13 J. D. Wang, G. Senette, Y. Tian and A. Clearfield, *Appl. Clay Sci.*, 1995, **10**, 103.
14 S. Kikkawa and M. Koizumi, *Mater. Res. Bull.*, 1982, **17**, 191.
15 C. Depège, L. Bigey, C. Forano, A. de Roy and J. P. Besse, *J. Solid State Chem.*, 1996, **126**, 314.
16 M. Ménétrier, K. S. Han, L. Guerlou-Depourgues and G. Delmas, *Inorg. Chem.*, 1997, **36**, 2441.
17 M. del Arco, V. Rives and R. Trujillano, *Stud. Surf. Sci. Catal.*, 1994, **87**, 507.
18 T. Sato, H. Fujita, T. Endo, M. Shimala and A. Tsunashima, *React. Solids*, 1988, **5**, 219.
19 M. A. Ulibarri, J. M. Fernández, F. M. Labajos and V. Rives, *Chem. Mater.*, 1991, **3**, 626.
20 J. M. Fernández, C. Barriga, M. A. Ulibarri, F. M. Labajos and V. Rives, *J. Mater. Chem.*, 1994, **4**, 1117.
21 JCPDS: Joint Committee on Powder Diffraction Standards, International Centre for Diffraction Data, Pennsylvania, 1977.
22 F. Rey, V. Fornés and J. M. Rojo, *J. Chem. Soc., Faraday Trans.*, 1992, **88**, 2233.
23 F. M. Labajos, V. Rives and M. A. Ulibarri, *J. Mater. Sci.*, 1992, **27**, 1546.
24 L. Pesic, S. Salipurovic, V. Markovic, W. Kagunya and W. Jones, *J. Mater. Chem.*, 1992, **2**, 1069.
25 M. del Arco, C. Martín, I. Martín, V. Rives and R. Trujillano, *Spectrochim. Acta, Part A*, 1993, **49**, 1575.
26 S. Miyata, *Clays Clay Miner.*, 1975, **23**, 369.
27 S. K. Yun and T. J. Pinnavaia, *Chem. Mater.*, 1995, **7**, 348.
28 M. A. Ulibarri, M. J. Hernández and J. Cornejo, *Thermochim. Acta*, 1987, **113**, 79.
29 B. C. Kruissink, L. van Reidjen and J. R. H. Ross, *J. Chem. Soc., Faraday Trans. 1*, 1981, **77**, 649.
30 K. Nakamoto, *Infrared and Raman Spectra of Inorganic and Coordination Compounds*, John Wiley & Sons, New York, 4th edn., 1986.
31 L. Tosi and J. Danon, *Inorg. Chem.*, 1964, **3**, 150.
32 S. Idemura, E. Suzuki and Y. Ono, *Clays Clay Miner.*, 1989, **37**, 553.
33 K. A. Carrado, A. Kostapapas and S. L. Suib, *Solid State Ionics*, 1988, **26**, 77.
34 F. A. P. Cavalcanti, A. Schutz and P. Biloen, in *Preparation of Catalysts IV*, eds. B. Delmon, P. Grange, P. A. Jacobs and G. Poncelet, Elseviere, Amsterdam, 1982, p. 165.
35 S. Miyata, *Clays Clay Miner.*, 1988, **31**, 305.
36 I. Crespo, C. Barriga, V. Rives and M. A. Ulibarri, *Solid State Ionics*, 1997, **101–103**, 729.
37 A. R. Champion and H. G. Drickamer, *J. Chem. Phys.*, 1967, **47**, 2592.
38 H. A. Larsen and H. G. Drickamer, *J. Phys. Chem.*, 1967, **61**, 1299.
39 M. Gordon, L. L. Williams and N. Sutin, *J. Am. Chem. Soc.*, 1961, **83**, 2061.
40 E. Pelizzetti, E. Mentasti and C. Baiocchi, *J. Phys. Chem.*, 1976, **80**, 2979.
41 L. H. Jones, *Inorg. Chem.*, 1963, **2**, 777.
42 H. B. Gray and N. A. Beach, *J. Am. Chem. Soc.*, 1963, **85**, 2922.
43 J. J. Alexander and H. B. Gray, *J. Am. Chem. Soc.*, 1968, **90**, 4260.
44 K. S. W. Sing, D. H. Everett, R. A. W. Haul, L. Moscou, R. Pierotti, J. Rouquerol and T. Sieminiewska, *Pure Appl. Chem.*, 1985, **57**, 603.
45 V. Rives, M. A. Ulibarri and A. Montero, *Appl. Clay Sci.*, 1995, **10**, 83.

Paper 8/04867C